Self-Driven Fractional Rotational Diffusion of the Harmonic Three-Mass System

Ori Saporta Katz and Efi Efrati*
Department of Physics of Complex Systems, Weizmann Institute of Science, Rehovot 76100, Israel

(Received 30 March 2018; published 16 January 2019)

In flat space, changing a system's velocity requires the presence of an external force. However, an isolated nonrigid system can freely change its orientation due to the nonholonomic nature of the angular momentum conservation law. Such nonrigid isolated systems may thus manifest their internal dynamics as rotations. In this work, we show that for such systems chaotic internal dynamics may lead to macroscopic rotational random walk resembling thermally induced motion. We do so by studying the classical harmonic three-mass system in the strongly nonlinear regime, the simplest physical model capable of zero angular momentum rotation as well as chaotic dynamics. At low energies, the dynamics are regular and the system rotates at a constant rate with zero angular momentum. For sufficiently high energies a rotational random walk is observed. For intermediate energies the system performs ballistic bouts of constant rotation rates interrupted by unpredictable orientation reversal events, and the system constitutes a simple physical model for Lévy walks. The orientation reversal statistics in this regime lead to a fractional rotational diffusion that interpolates smoothly between the ballistic and regular diffusive regimes.

DOI: 10.1103/PhysRevLett.122.024102

It is well known that deformable systems, such as cats, can rotate with zero angular momentum, by performing a cyclic sequence of internal deformations. This deformation-induced rotation (DIR) is a direct result of the nonholonomic constraint imposed on nonrigid bodies by the conservation of angular momentum [1]; as a result, the orientation of deformable systems is a history-dependent function of the system's shape deformations. Such systems have been studied extensively in the context of control theory, for example, in the study of falling cats [2] and of gymnastic maneuvers [3]. The dynamics of these systems are often formulated in terms of a gauge field on the space of free variables [4], the gauge freedom related to the ambiguity in defining the orientation of a deformable system. The history dependence of the nonholonomically constrained variables manifests in the accumulation of the relevant geometric phase, reminiscent of Berry's phase [5,6], along the trajectory of the system. In mechanical systems in particular, DIR allows the deformable system's orientation to serve as a sensitive measurable for the nature of the system's internal dynamics.

In this work, we exploit the dynamical variability of a mixed conservative system that can perform DIR and show that an extremely simple mechanical system in isolation can exhibit vastly different types of self-driven rotational motion. Specifically, we study the nonlinear dynamics of the harmonic three-mass system with finite rest lengths [Fig. 1(a)]. Three-body systems are the minimal systems capable of DIR as at least two distinct shape degrees of freedom are required to produce rotation. Similarly to the harmonic benzene molecular model [7], despite the purely harmonic interactions, geometric nonlinearities lead to positive Lyapunov exponents and chaotic dynamics for large enough strains [8]. For low-energy states the system behaves regularly as expected given the underlying pairwise harmonic interactions. We show that this mixed phase space is responsible for statistically distinct types of self-driven rotation, from regular motion through fractional diffusion to regular diffusion, determined almost solely by the energy of the system. In between the regular and diffusive limiting behaviors, we observe sticking dynamics typical of mixed systems [15]. This gives rise to anomalous diffusion characterized by fractional exponents and constitutes a simple mechanical model for Lévy walks.

Despite the relatively high dimension of its phase space, the statistics of the dynamics are determined almost solely by the energy of the system. Thus, the rotational statistics provide a sensitive measurable for the type of dynamics

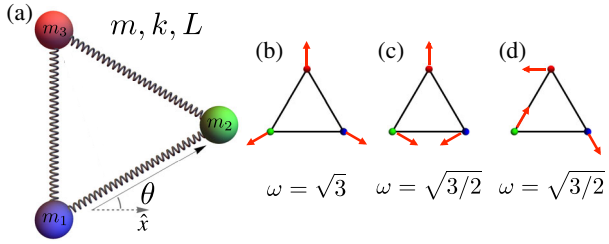

FIG. 1. The symmetric harmonic three-mass system. (a) Sketch of the system with equal masses m, spring constants k, and rest lengths L. θ is the angle between r_{12} and the x axis, used to determine the orientation of the three-mass triangle. Panels (b)–(d) present the normal modes and corresponding frequencies, commonly known as the symmetric stretch, isometric bend, and asymmetric bend, respectively.

while the energy serves as a robust control parameter through which the transition from regularity to chaos and the origin of fractional statistics in mixed autonomous Hamiltonian systems can be studied.

The harmonic three-mass system is described by the autonomous Hamiltonian,

$$\mathcal{H} = \sum_{i=1}^{3} \frac{\mathbf{p}_i^2}{2m_i} + \sum_{\langle ij \rangle} \frac{k_{ij}}{2}(r_{ij} - L_{ij})^2, \tag{1}$$

where $\mathbf{r}_{ij} = \mathbf{r}_i - \mathbf{r}_j$, and $r_{ij} = |\mathbf{r}_{ij}| \equiv \sqrt{\mathbf{r}_{ij} \cdot \mathbf{r}_{ij}}$.

We consider only motions of zero total angular momentum. Thus, the motion is constrained to a plane [16], and it suffices to analyze the problem in two dimensions. The geometric nonlinearities originating from the nonvanishing rest lengths of the harmonic springs manifest algebraically in the square root in the potential term and break the integrability of the system [7,8].

The system's dynamics are studied using a symplectic numerical integrator; see Supplemental Material (SM) for details [8]. The parameters are chosen to be uniform for all the masses and springs: $m_i = 1$, $k_{ij} = 1$, and $L_{ij} = 2$, and the corresponding equilibrium state of the system is an equilateral triangle. The typical timescale is $\tau_s = \sqrt{m/k} = 1$ and the reference energy scale is $E_s = 3/2kL^2 = 6$, which corresponds to the elastic energy required to shrink the triangle to a point. All the initial conditions prescribed to the system have zero angular and linear momentum, and are obtained by determining the amplitudes and relative phases of the normal modes in the shape variables [17]. Simulating the system for a variety of initial conditions spanning a wide range of energies, we identified four qualitatively distinct types of trajectories, approximately corresponding to four energy regimes. The time evolution of the orientation of the three-mass triangle for each of these four types of trajectories is depicted in Fig. 2.

Initial conditions of very small energies $E \ll 1$ result in regular oscillatory motion superimposed on rotation with a constant average angular velocity [Fig. 2(a)]. The normal modes of motion in this regime seem harmonic and noninteracting, and naively one could attempt to linearize the Hamiltonian about a particular rest configuration of the spring-mass triangle. This textbook-type exercise [19] yields frequencies that agree with the observed frequencies, yet it predicts oscillations about a specific state and fails to produce a constant average angular velocity.

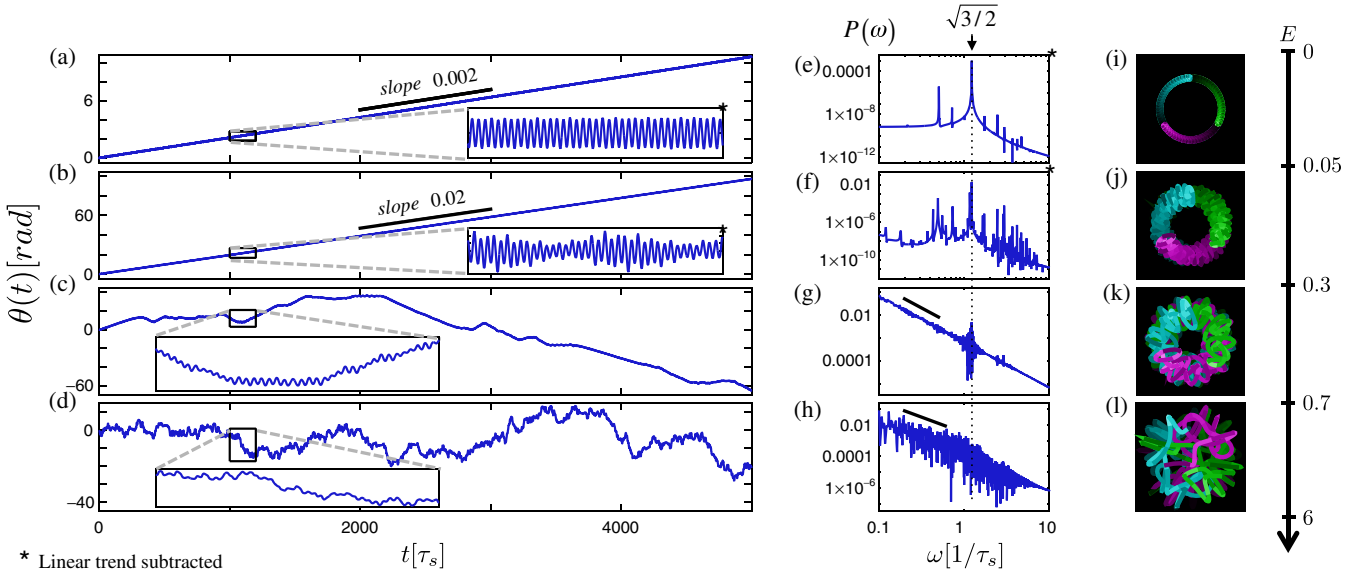

FIG. 2. Four typical trajectories of the orientation of the three-mass triangle as a function of time (a)–(d), their power spectra (e)–(h), and a long-exposure image of their dynamics with each mass colored in a different color (i)–(l). The initial conditions differ in energies: (a),(e),(i) $E = 0.02$, (b),(f),(j) $E = 0.28$, (c),(g),(k) $E = 0.62$, (d),(h),(l) $E = 1.29$. The energy units fit the simulation parameters $m = 1$, $L = 2$, $k = 1$ for which the typical energy scale reads $E_s = 3kL^2/2 = 6$. (a),(e),(i) At low energies $E \ll 1$, the system behaves quasiperiodically, with frequencies fitting the linear modes of the system, peaking at the degenerate linear frequency $\sqrt{3/2}$. (b),(f),(j) At slightly higher energies $0.05 \lesssim E \lesssim 0.3$, the degenerate frequencies split, leading to beating, and the system displays nonlinear yet regular oscillations. (c),(g),(k) At higher energies $0.3 \lesssim E \lesssim 0.7$, the system becomes observably chaotic, exhibiting quasiperiodic motion on short timescales, and unpredictable transitions between constant angular velocity bouts on long timescales that show high sensitivity to initial conditions. The power spectrum fills up, adopting a constant ω^{-2} slope yet continues to display a significant peak around the linear frequency $\sqrt{3/2}$. (d),(h),(l) Around the energy $E \gtrsim 0.7$, the system loses its short-time periodicity and the orientation resembles a random walk. The power spectrum shows that all frequencies are excited with approximately the same power, and the linear frequencies lose significance.

In order to properly capture the motion of the spring-mass system, a reduced description that does not restrict the dynamics of the system is necessary, as has been carried out for general three-body systems in several works [20–23]. The reduction process consists of describing the system as a deforming triangle placed in the plane instead of as three masses moving independently. From the rotational symmetry of the problem, only the velocity of the orientation variable appears in the equations, and can be reduced by setting the angular momentum to zero. In our case, the reduced Hamiltonian reads

$$H_{\mathrm{red}} = w(p_1^2 + p_2^2 + p_3^2) + \sum_{\langle ij \rangle} \frac{k}{2}(r_{ij}(\boldsymbol{w}) - L)^2, \qquad (2)$$

where

$$w = |\boldsymbol{w}|, \quad p_i = \frac{\dot{w}_i}{2w}, \quad r_{ij}(\boldsymbol{w}) = \sqrt{2(w - \boldsymbol{w}\cdot\boldsymbol{b}^{ij})},$$
$$\boldsymbol{b}^{13} = \left(\frac{1}{2}, \frac{\sqrt{3}}{2}, 0\right), \quad \boldsymbol{b}^{12} = (-1, 0, 0), \quad \boldsymbol{b}^{23} = \left(\frac{1}{2}, -\frac{\sqrt{3}}{2}, 0\right).$$

The shape variables $\boldsymbol{w} = (w_1, w_2, w_3)$, presented in Refs. [17,18] for three-body systems, are a Bloch sphere representation of the two relative Jacobi coordinates of the three masses, and the p_i's are their canonically conjugate momenta. The orientation variable θ describes the angle formed between the line connecting m_1 and m_2 and the x axis. The center-of-mass coordinates decouple from the rest of the system and are set to zero.

Expanding the reduced Hamiltonian Eq. (2) about its equilibrium shape, the resulting dynamics describe the low-energy dynamics well. Unlike the small displacement approximation, in the present case calculating the full motion resulting from these oscillations yields a non-vanishing averaged angular velocity given, to first non-vanishing order, by

$$\bar{\dot{\theta}} = \frac{1}{16}\sqrt{\frac{3}{2}} A_1 A_2 \sin(\Delta\varphi), \qquad (3)$$

where A_1 and A_2 are the amplitudes of the two degenerate normal modes, the symmetric stretch and the isometric bend, and $\Delta\varphi \equiv \varphi_1 - \varphi_2$ is the phase difference between them, and determines the direction of rotation. This zero angular momentum ratcheting motion is a direct outcome of the spectrum's degeneracy, resulting from the symmetries of the system. Equation (3) was first derived in Ref. [22] for infinitesimal perturbation of a collinear molecule assuming degenerate frequencies. In our case the degeneracy is a direct result of the details of the linearized system.

It is somewhat surprising that the constant average angular velocity persists at higher energies, where the degeneracy breaks, the oscillations become nonlinear, and the angular motion displays beating. Indeed, in the quasiperiodic nonlinear regime, typical for $0.05 \lesssim E \lesssim 0.3$ [Fig. 2(b)], the prediction of the averaged angular velocity Eq. (3) increasingly deviates from the one observed numerically as the energy is increased and the interaction between the modes becomes more pronounced. These nonlinear oscillations are explained by the Kolmogorov-Arnold-Moser theorem, which predicts the persistence of regular trajectories in almost-integrable systems. Their frequencies are well captured by Birkhoff normal form theory, presented in Ref. [24] and applied to the harmonic three-body system in Ref. [25], where the beating observed in the dynamics of θ is identified with periodic energy transfer between the degenerate modes.

For moderate energies $0.3 \lesssim E \lesssim 0.7$, the regular nature of the dynamics of the system breaks for most initial conditions, manifesting in the "filling up" of the spectrum observed in Fig. 2(g). For short times the motion is reminiscent of the regular motion observed for lower energy, but portrays some irregularities. After a finite time the direction of the rotation abruptly reverses and the system rotates, again with a constant average angular velocity, in the opposite direction. This sticking of chaotic trajectories to quasiperiodic trajectories for long times is typical of mixed systems. Aside from the transition regions, the motion remains very close to the quasiperiodic trajectories explaining the peak of the power spectrum around $\omega = \sqrt{3/2}$ [Fig. 2(g)].

The durations of the constant velocity bouts are highly sensitive to initial conditions, and for energies at the lower limit of this regime the tail of their probability density function (PDF) fits a power law: $P(\tau) \propto \tau^{-\nu-1}$. This fits the setting of the stochastic Lévy-walk model [26] used to describe anomalous sub- and superdiffusive phenomena in systems ranging from quantum transport [27], through turbulence [28], to biological locomotion [29]. For values of $1 < \nu < 2$, the model predicts an angular mean-squared displacement (MSD) exponent $\langle\theta^2\rangle \propto t^\alpha$ that satisfies $\alpha = 3 - \nu$. In our system, near the loss of integrability the obtained values of ν are close to 1 and α follows this prediction well (Fig. 3). However, as the energy is increased, the bout length PDF exponent ν increases away from 1 and the fit to a clean power law deteriorates. In this regime α also deviates from the Lévy-walk predicted value, yet it continues to decrease monotonically.

The mechanism behind these power-law sticking time statistics in Hamiltonians, observed in various mixed systems [30,31], has not been completely elucidated. For low-dimensional systems $d \leq 2$, a quantitative model has been formulated [32] and shown to accurately predict the MSD anomalous exponent [33,34], but for higher-dimensional systems (such as ours) the mechanism is still unresolved [35].

As the energy rises, the constant average angular velocity bout times shorten until at sufficiently high energies, $0.7 \lesssim E \lesssim 6$, the linear frequencies disappears [Fig. 2(d)]

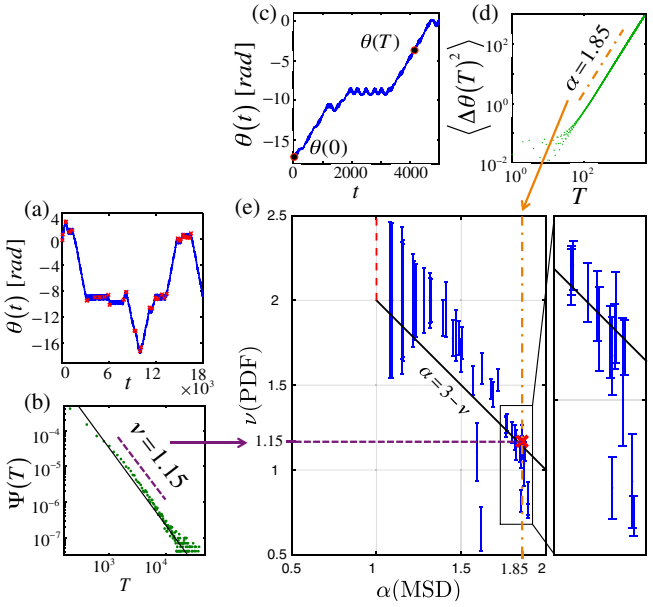

FIG. 3. Comparison between the angular MSD and the bout-length PDF in the regime of motion $0.3 \lesssim E \lesssim 0.7$, where the motion is composed from bouts of constant averaged angular velocity of varying times. Panels (a) and (b) show the process of calculating the bout-length PDF, $\Psi(T)$, for a trajectory with $E = 0.31$ by identifying the turning points between segments of constant averaged angular velocity. Panel (a) shows the given trajectory with red asterisks marking the turning points identified by the algorithm. Panel (b) shows the resulting $\Psi(T)$ in a log-log plot along with the linear fit. Panels (c) and (d) show the process of calculating the MSD for the same trajectory, by averaging $[\theta(T) - \theta(0)]^2$ over 10^4 runs (see SM [8]). When T is big enough, the MSD is an excellent fit to a power law $\langle \Delta\theta(T)^2 \rangle \propto T^\alpha$ with an anomalous diffusion exponent α, as depicted in (d). (e) The PDF power ν as a function of the anomalous diffusion exponent α for several initial conditions in the relevant energy range $0.3 \lesssim E \lesssim 0.7$. The black solid line and red dotted line show the Lévy-walk model prediction, $\alpha = 3 - \nu$. For the lower energies $E \approx 0.3$ (the enlarged region) the two exponents follow the Lévy-walk prediction well. As the energy grows, the average bout length shortens and α decreases, changing from almost 2 to 1 at high enough energies, $E \gtrsim 0.7$. The PDF fit to a single power law gradually deteriorates with increasing energy and we observe significant deviations from the power-law-based Lévy-walk prediction.

and the MSD exponent satisfies $\alpha = 1$, characterizing a standard random walk. This deterministic regular diffusion results from a sufficiently rapid memory loss of the initial conditions due to the chaotic dynamics. However, chaos and deterministic diffusion are not directly related; non-chaotic systems may exhibit diffusion [36], while chaotic dynamics may fail to produce regular diffusion, such as in the intermediate energy regime of our system: although the largest Lyapunov exponent is positive [8], the diffusion is anomalous. While the MSD in this regime resembles the result of a Wiener process [37], it is the outcome of a relatively low-dimensional deterministic chaotic process rather than resulting from stochastic noise associated with a diverging Kolmogorov-Sinai entropy [38]. Moreover, much like in the Fermi-Pasta-Ulam system, it is unclear if the system reaches thermal equilibrium and equipartition [38]. The deviation of higher order moments of the angular displacement from the expected linear relation of an uncorrelated random walk model (see SM [8]) indicates that some correlations are retained.

The lowest energy for which $\alpha = 1$ is only slightly above the threshold energy for collinear configurations $E = 2/3$ (Fig. 4). Collinear configurations followed by orientation reversal of the spring-mass triangle, which are rare at $E \gtrsim 2/3$, become more and more frequent as the energy is increased. However, the angle θ is still well defined, and strobing its value only whenever the triangle returns close enough to its original unreflected shape (up to similarities) produces the same statistics.

The harmonic three-mass problem shows a remarkable variety of behaviors with the total energy content of the system as the main control parameter. As the system is mixed, islands of regular behavior are found for every value of the total energy in the system; however, they become small fast as the energy is increased. This allows us to study

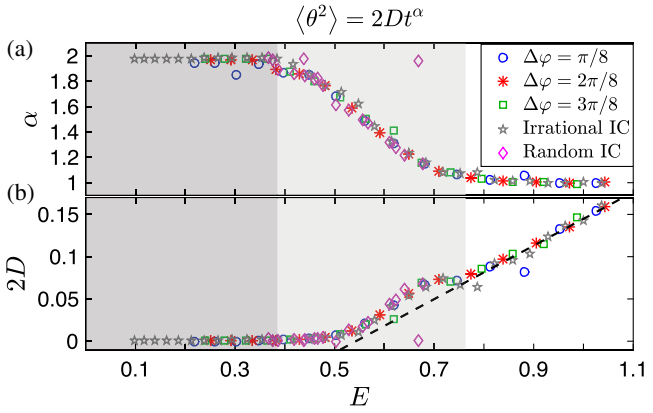

FIG. 4. The diffusion exponent α (a) and diffusion coefficient D (b) satisfying $\langle \theta^2 \rangle = 2Dt^\alpha$ plotted as a function of the energy for various types of initial conditions (IC). Error bars are smaller than the symbols. The (blue) circle, (red) asterisk, and (green) square symbol correspond to initial conditions set by different phase differences between the degenerate modes. The (gray) pentagram plot corresponds to irrational initial phase difference. The (magenta) diamond plot corresponds to random initial conditions. For most initial conditions the energy suffices for predicting α. Near $E = 0.35$ trajectories begin to change from ballistic angular motion where $\alpha = 2$ (dark gray background) to anomalous diffusion, where $1 < \alpha < 2$ (light gray background), and at around $E = 0.7$ trajectories begin to change to regular diffusion (clear background), where $\alpha = 1$. In this regime, the diffusion coefficient appears to be linear in the energy with a slope 0.32 and an offset at $E \approx 0.5$. The MSD is calculated by averaging over a large ensemble of similar initial conditions; see SM for details [8].

a typical behavior for every energy value, manifesting in the data collapse of the fractional diffusion exponent α and of the diffusion coefficient D as a function of the energy for a variety of initial conditions (Fig. 4). The mechanical simplicity of the system makes it a viable option for experimental realization of Lévy walks and stochastic orientation reversals, if the numerically observed phenomena can survive friction.

As the evolution of the nonholonomic variable depends on the full history of the dynamics of the independent variables in the system, it serves as an exceptionally good proxy for temporal correlations between the independent variables. We argue that in general, whenever probing the dynamics of a nonholonomically constrained variable in a mixed Hamiltonian system, such fractional statistics are to be expected. Within the regular trajectories the constrained variable will propagate ballistically. As the chaotic domains grow, stochastic transitions between such ballistic bouts will occur and the long-time correlations in these trajectories will manifest as fractional statistics for the values of the nonholonomically constrained variable. Finally, deep in the chaotic regime one expects correlations to be very short-lived and give rise to a regular random walk.

For example, consider the gravitational three-body system in uniformly curved space in which it was shown that nonrigid bodies can translate with no linear momentum [39,40]. We predict that a chaotic gravitational three-mass dynamics in curved space will manifest as real space diffusion, much like chaotically excited surface adsorbed molecules [7,41], realizing Brown's initial interpretation of a random walk as belonging to the particle itself [42]. The exact nature of this motion is yet to be explored.

E. E. would like to thank Steve Tse, Ramis Movassagh, and Tom Witten for helpful discussions on exploring the three-mass system. The authors would also like to acknowledge helpful discussions with Shmuel Fishman, Or Alus, Dmitry Turaev, Norman Zabusky, Yannis Kevrekidis, Kevin Mitchell, and Eli Barkai. This work was supported by the ISF Grant No. 1479/16. E. E. thanks the Ascher foundation for their support, and also acknowledges the support by the Alon fellowship.

*efi.efrati@weizmann.ac.il

[1] A. Guichardet, Ann. Inst. Henri Poincaré **40**, 329 (1984).
[2] R. Montgomery, Fields Inst. Commun. **1**, 193 (1993).
[3] C. Frohlich, Sci. Am. **242**, No. 3, 154 (1980).
[4] R. W. Batterman, Stud. Hist. Philos. Sci. Part B **34**, 527 (2003).
[5] F. Wilczek and A. Shapere, *Geometric Phases in Physics* (World Scientific, Singapore, 1989), Vol. 5.
[6] M. V. Berry, Proc. R. Soc. London, Ser. A **392**, 45 (1984).
[7] A. S. De Wijn and A. Fasolino, J. Phys. Condens. Matter **21**, 264002 (2009).
[8] See Supplemental Material at http://link.aps.org/supplemental/10.1103/PhysRevLett.122.024102 for additional information about the simulation methods and the techniques used to calculate the mean-squared displacement and probability density function, which includes Refs. [9–14].
[9] K. Ramasubramanian and M. Sriram, Physica (Amsterdam) **139D**, 72 (2000).
[10] A. Wolf, J. B. Swift, H. L. Swinney, and J. A. Vastano, Physica (Amsterdam) **16D**, 285 (1985).
[11] E. Hairer and G. Wanner, in *Encyclopedia of Applied and Computational Mathematics* (Springer, New York, 2015), pp. 451–455.
[12] L.-S. Yao, Nonlinear Anal. Model. **15**, 109 (2010).
[13] V. Zaburdaev, S. Denisov, and J. Klafter, Rev. Mod. Phys. **87**, 483 (2015).
[14] E. Bouchbinder, I. Procaccia, S. Santucci, and L. Vanel, Phys. Rev. Lett. **96**, 055509 (2006).
[15] G. Zaslavsky and M. Edelman, Chaos **10**, 135 (2000).
[16] E. T. Whittaker, *A Treatise on the Analytical Dynamics of Particles and Rigid Bodies* (Cambridge University Press, Cambridge, England, 1988).
[17] These variables were first presented in [18]. They are explicitly given by

$$w_1 = \frac{m}{6}(|\mathbf{r}_{23}|^2 + |\mathbf{r}_{13}|^2 - 4\mathbf{r}_{23}\cdot\mathbf{r}_{13}),$$
$$w_2 = \frac{m}{2\sqrt{3}}(|\mathbf{r}_{23}|^2 - |\mathbf{r}_{13}|^2),$$
$$w_3 = \frac{m}{\sqrt{3}}(\mathbf{r}_{13}\wedge\mathbf{r}_{23}).$$

[18] T. Iwai, J. Math. Phys. (N.Y.) **28**, 1315 (1987).
[19] G. L. Kotkin and V. G. Serbo, *Collection of Problems in Classical Mechanics* (Pergamon Press, New York, 1971), Vol. 31, pp. 179–182.
[20] R. Montgomery, Am. Math. Mon. **122**, 299 (2015).
[21] R. G. Littlejohn and M. Reinsch, Rev. Mod. Phys. **69**, 213 (1997).
[22] T. Iwai and H. Yamaoka, J. Phys. A **38**, 5709 (2005).
[23] J. E. Marsden, T. S. Ratiu, and J. Scheurle, J. Math. Phys. (N.Y.) **41**, 3379 (2000).
[24] D. Bambusi, An introduction to Birkhoff normal form. Universita di Milano, 2014, http://users.mat.unimi.it/users/bambusi/pedagogical.pdf.
[25] O. Saporta Katz and E. Efrati, Integrable dynamics for low and moderate energy in the harmonic three body system (to be published).
[26] T. Geisel, in *Lévy Flights and Related Topics in Physics* (Springer, New York, 1992), pp. 151–173.
[27] S. F. Lee and M. A. Osborne, Chem. Phys. Chem. **10**, 2174 (2009).
[28] M. F. Shlesinger, B. J. West, and J. Klafter, Phys. Rev. Lett. **58**, 1100 (1987).
[29] G. Ariel, A. Rabani, S. Benisty, J. D. Partridge, R. M. Harshey, and A. Be'Er, Nat. Commun. **6**, 8396 (2015).
[30] F. Cagnetta, G. Gonnella, A. Mossa, and S. Ruffo, Europhys. Lett. **111**, 10002 (2015).
[31] V. Latora, A. Rapisarda, and S. Ruffo, Phys. Rev. Lett. **83**, 2104 (1999).

[32] J. D. Meiss and E. Ott, Physica (Amsterdam) **20D**, 387 (1986).
[33] O. Alus, S. Fishman, and J. D. Meiss, Phys. Rev. E **90**, 062923 (2014).
[34] O. Alus, S. Fishman, and J. D. Meiss, Phys. Rev. E **96**, 032204 (2017).
[35] S. Lange, A. Bäcker, and R. Ketzmerick, Europhys. Lett. **116**, 30002 (2016).
[36] E. Hauge and E. Cohen, J. Math. Phys. (N.Y.) **10**, 397 (1969).
[37] N. G. Van Kampen, *Stochastic Processes in Physics and Chemistry*, 3rd ed. (Elsevier, New York, 1992), Vol. 1, pp. 78–81.
[38] G. Gallavotti, *The Fermi-Pasta-Ulam Problem: A Status Report* (Springer, New York, 2007), Vol. 728.
[39] J. Wisdom, Science **299**, 1865 (2003).
[40] J. Avron and O. Kenneth, New J. Phys. **8**, 68 (2006).
[41] S. Hallerberg and A. S. de Wijn, Phys. Rev. E **90**, 062901 (2014).
[42] R. Brown, Philos. Mag. **4**, 161 (1828).